Separable model for the antinucleon-nucleon elastic and annihilation interaction

W. Schweiger, J. Haidenbauer, and W. Plessas
Institut für Theoretische Physik, Karl-Franzens-Universität Graz, A-8010 Graz, Austria
(Received 13 March 1985)

In the framework of a coupled-channel approach we construct a separable potential model for the low- and medium-energy antinucleon-nucleon interaction. The elastic part is derived from the meson-exchange Paris potential and represented in an on-shell and off-shell equivalent separable form. In analogy to microscopic theories the annihilation interaction is also described by a separable potential but with phenomenological form factors. Coulomb corrections to the hadronic interaction are taken into account rigorously. We present results for total, elastic, and charge-exchange cross sections and compare them to existing experimental data at low and medium energies. A first application of the model to the calculation of hadronic level shifts in antiprotonic hydrogen is reported.

I. INTRODUCTION

One appealing motivation to study the antinucleon-nucleon ($\bar{N}$-N) interaction is the fact that the sophistication reached in describing the nucleon-nucleon (N-N) force[1] can be immediately transferred to $\bar{N}$-N potentials via the G-parity transformation. As a consequence of this relation particular (spin-dependent) components of the hadronic interaction play distinct roles in the N-N and $\bar{N}$-N systems. Therefore it should also be possible to obtain additional evidence on meson-exchange dynamics from $\bar{N}$-N data. This aim, however, is considerably impeded by the occurrence of $\bar{N}$-N annihilation and demands for a detailed understanding of the underlying processes. Attempts that account for $\bar{N}$-N annihilation can be divided into three categories: purely phenomenological, semiphenomenological, and microscopic models. We will only quote their main characteristics, since in recent times several review papers dealt with this subject.[2]

In purely phenomenological models the annihilation is taken into account just via an *ad hoc* optical potential.[3,4] Semiphenomenological models in addition include some notions from microscopic theories such as radial shape of the annihilation potential from meson theory[5] or bag models[6] and/or they pay regard to the multichannel situation by explicitly introducing one or more effective decay channels;[7,8] most suitably this can be achieved by a coupled-channel approach, which then provides for a more realistic energy-dependence of the annihilation. However, a detailed understanding of the annihilation mechanism leading to specific mesonic channels requires microscopic theories. Essentially two different concepts have been developed. The one is based on meson theory,[9] while the other describes the annihilation in the quark picture. The simplest approach motivated by quantum chromodynamics assumes a quark-antiquark (q-$\bar{q}$) pair to annihilate into a gluon (g). The resulting $q^2\bar{q}^2g$ state is considered as a "doorway" to the various meson channels.[6,10,11] Another microscopic model, which already allows for the prediction of branching ratios, relies on quark rearrangement.[12–14] A further refinement consists in the addition of quark-antiquark annihilation,[15,16] but it is still an open question which processes are most important.[17] In the quark-rearrangement model one can determine the coupling to the meson channels via the overlap of the $\bar{q}^3q^3$ wave function of the $\bar{N}$-N system with the $\bar{q}q$ meson wave functions. In the particular approach followed by Green *et al.*[13] an overall coupling strength remains the only open parameter. Assuming a harmonic oscillator confinement potential, one is left with Gaussian wave functions, which then lead to separable coupling potentials. In its most elaborate version (including P waves, Δ intermediate states, and meson widths) this model is able to describe up to 70% of the annihilation at $E_{\rm lab}\approx 100$ MeV, say. However, we are still far away from an adequate description of the complete $\bar{N}$-N interaction. For example, the annihilation models themselves differ considerably with respect to their range and the interplay with the elastic $\bar{N}$-N interaction is also not clear. Furthermore, the latter is sometimes oversimplified (e.g., by neglecting velocity dependence) or described unsatisfactorily, especially at smaller distances.

In order to examine specific details of the $\bar{N}$-N interaction in the $\bar{N}$-N problem and few-body as well as nuclear applications, we aimed at a careful description of the $\bar{N}$-N system, which should allow for a clear distinction of the various effects. Motivated by the fact that a major part of the interaction results in separable form from the treatment of the annihilation in microscopic theories,[12,13] we attempted to describe the whole $\bar{N}$-N interaction by a separable potential. Such a model readily lends itself to application in a coupled-channel formalism even of high dimension. Earlier shortcomings of separable interactions are overcome by now, since suitable approximation schemes have made it possible to represent any given two-body interaction in separable form while preserving all essential properties.[18] Just recently a separable parametrization of the meson-theoretical N-N potential of the Paris group[1] was presented reproducing both the on-shell and off-shell characteristics rather accurately.[19] This approach for the first time allows us to introduce a genuine meson-exchange N-N model to three-nucleon scattering.[20]

For the $\bar{N}$-N interaction we proceeded in a similar way.

First we chose the G-parity transformed Paris N-N interaction for the elastic $\bar{N}$-N potential[5] and cast it into an off-shell equivalent separable form. Once a reliable elastic part of the $\bar{N}$-N interaction was established, we added in a coupled-channel framework one effective two-particle decay channel per isospin state. In accordance with the foregoing discussion we assumed the coupling potentials to be separable. This approach is certainly superior to simply fitting a local optical potential by a separable ansatz[21] since it provides for a more fundamental meson-exchange elastic part and allows us to clearly isolate the annihilation interaction.

A reliable separable model for the $\bar{N}$-N interaction is highly desired for applications in antinucleonic few-body systems and $\bar{N}$-nucleus scattering. For example, in an $\bar{N}$-nucleus optical potential the off-shell two-particle ($\bar{N}$-N) transition matrix has to be folded with the nuclear density, which can be done in an easier way with separable potentials. Three-body problems with refined N-N respectively $\bar{N}$-N interactions in subsystems can only be solved via separable potentials.[20] In addition, the Coulomb interaction can be treated rigorously in connection with a separable hadronic force.[22] This is of great importance in calculating atomic levels (shifts and widths) of antiprotonic atoms and also for a proper description of the nuclear antiproton-proton ($\bar{p}$-p) system.

In the following section we shall outline the coupled-channel formalism for $\bar{N}$-N scattering including Coulomb and neutron-proton (n-p) mass-difference corrections. In Sec. III our separable interaction model will be presented. Section IV will contain a discussion of results we obtained for $\bar{N}$-N scattering observables and hadronic level shifts of antiprotonic hydrogen. After the Conclusion some general properties of separable annihilation potentials are summarized in the Appendix.

II. FORMALISM

If Coulomb and n-p mass-difference corrections are to be included, the $\bar{N}$-N system is most conveniently treated in the charge representation. Its basis consists of the states $|\bar{p}p\rangle$ and $|\bar{n}n\rangle$ representing the antiproton-proton and antineutron-neutron channels, respectively; they are coupled, if the hadronic interaction is isospin dependent. The relation of these states to the isospin eigenstates $|I,m_I\rangle$ is given by the unitary transformation

$$\begin{pmatrix} |\bar{p}p\rangle \\ |\bar{n}n\rangle \end{pmatrix} = U \begin{pmatrix} |1,0\rangle \\ |0,0\rangle \end{pmatrix} \tag{2.1a}$$

with

$$U = \frac{1}{\sqrt{2}} \begin{pmatrix} 1 & 1 \\ -1 & 1 \end{pmatrix} . \tag{2.1b}$$

Since the strong interaction is assumed to be isospin invariant, the potential matrix containing the isospin 1 and isospin 0 potentials V_S^1 and V_S^0, respectively,

$$\mathscr{V}_S^I = \begin{pmatrix} V_S^1 & 0 \\ 0 & V_S^0 \end{pmatrix} \tag{2.2}$$

is diagonal in the isospin basis. We use superscripts "*ch*" and "*I*" to indicate the particular representations. Notice that the isospin channels $|0,0\rangle$ and $|1,0\rangle$ decouple when Coulomb and n-p mass-difference effects are neglected. Adding the annihilation interaction increases the dimension of the matrix $\mathscr{V}_S^I$. For the simplest case of one decay channel per isospin state and noninteracting decay products it takes the particular form

$$\mathscr{V}_S^I = \begin{pmatrix} V_S^1 & V_a^{1\dagger} & 0 & 0 \\ V_a^1 & 0 & 0 & 0 \\ 0 & 0 & V_S^0 & V_a^{0\dagger} \\ 0 & 0 & V_a^0 & 0 \end{pmatrix} , \tag{2.3}$$

where coupling to the annihilation channels is caused by the interactions V_a^I. If one is interested in the overall influence of the annihilation on the $\bar{N}$-N sector, one can derive an optical potential by formally solving the integral equations for the transition operators into the decay channels. This is easily done in case there is no interaction between the decay products and results in an effective potential

$$\mathscr{V}_{\rm opt}^I = \begin{pmatrix} V_{\rm opt}^1 & 0 \\ 0 & V_{\rm opt}^0 \end{pmatrix} , \tag{2.4a}$$

where

$$V_{\rm opt}^I = V_S^I + V_a^{I\dagger}(E - E^I - h_0^I + i0)^{-1} V_a^I, \quad (I=0,1) . \tag{2.4b}$$

The operators h_0^I denote the free Hamiltonians in the decay channels ($I=0,1$) and the energies E^I their thresholds.

For the inclusion of the Coulomb interaction V_C we pass over to the charge representation by means of the transformation U of Eq. (2.1b). The total potential in the $\bar{N}$-N sector then reads

$$\mathscr{V}^{\rm ch} = \mathscr{V}_C^{\rm ch} + \mathscr{V}_{\rm opt}^{\rm ch} \tag{2.5a}$$

with

$$\mathscr{V}_C^{\rm ch} = \begin{pmatrix} V_C & 0 \\ 0 & 0 \end{pmatrix} , \tag{2.5b}$$

$$\mathscr{V}_{\rm opt}^{\rm ch} = \tfrac{1}{2} \begin{pmatrix} V_{\rm opt}^0 + V_{\rm opt}^1 & V_{\rm opt}^0 - V_{\rm opt}^1 \\ V_{\rm opt}^0 - V_{\rm opt}^1 & V_{\rm opt}^0 + V_{\rm opt}^1 \end{pmatrix} . \tag{2.5c}$$

From now on we shall only work in the charge representation and therefore omit the superscripts "ch."

Allowing for spin-dependent but rotational invariant forces one can perform a partial-wave decomposition. A novel feature as compared to the N-N system is the possibility of coupling spin singlet and spin triplet for angular momentum states ${}^{2S+1}L_J$ with $L=J$. If one assumes the whole elastic part of the $\bar{N}$-N interaction to be derived from the N-N system by the G-parity transformation, such transitions can only occur via mesonic intermediate states. Since they only take place for higher partial waves (${}^1P_1 \leftrightarrow {}^3P_1$, ${}^1D_2 \leftrightarrow {}^3D_2$, etc.) their importance is presumably small at low and medium energies and we can consider

the spin to be conserved. Then in addition to the coupling of the particle states $|\bar{p}p\rangle$ and $|\bar{n}n\rangle$ we have only the coupling of angular momentum states $l_<=J-1$ and $l_>=J+1$. For fixed total angular momentum J the potential (2.5a) reads

$$\mathscr{V}^J=\mathscr{V}^J_C+\mathscr{V}^J_{\rm opt}\ , \tag{2.6}$$

where

$$\mathscr{V}^J_C=\begin{bmatrix}\mathbf{V}_C & 0\\ 0 & 0\end{bmatrix} \tag{2.7a}$$

with

$$\mathbf{V}_C=\begin{bmatrix}V_{Cl_<} & 0\\ 0 & V_{Cl_>}\end{bmatrix} \tag{2.7b}$$

and

$$\mathscr{V}^J_{\rm opt}=\tfrac{1}{2}\begin{bmatrix}\mathbf{V}^0_{\rm opt}+\mathbf{V}^1_{\rm opt} & \mathbf{V}^0_{\rm opt}-\mathbf{V}^1_{\rm opt}\\ \mathbf{V}^0_{\rm opt}-\mathbf{V}^1_{\rm opt} & \mathbf{V}^0_{\rm opt}+\mathbf{V}^1_{\rm opt}\end{bmatrix} \tag{2.7c}$$

with

$$\mathbf{V}^I_{\rm opt}=\begin{bmatrix}V^I_{{\rm opt},l_<l_<} & V^I_{{\rm opt},l_<l_>}\\ V^I_{{\rm opt},l_>l_<} & V^I_{{\rm opt},l_>l_>}\end{bmatrix},\quad (I=0,1)\ . \tag{2.7d}$$

For angular momentum decoupling $l_<=l_>=L=J$ the above matrices $\mathbf{V}$ reduce to the corresponding partial-wave potentials V_{CL} and $V^I_{{\rm opt},L}$, respectively.

Up until now we have not restricted the spin structure of the decay channel. Assuming spinless decay products conservation of J implies

$$V^I_{{\rm opt},LL'}=V^I_{S,LL'}+V^{I\dagger}_{a,JL}(E-E^I-h^I_{0,J}+i0)^{-1}V^I_{a,JL'}\ , \quad (I=0,1) \tag{2.8}$$

for $L,L'=l_<,l_>$.

Next we demonstrate the solution of the $\bar{\rm N}$-N scattering problem for the Coulomb plus strong potential $\mathscr{V}^J$ in Eq. (2.6) by applying the Gell-Mann-Goldberger two-potential formalism.[23] For the total transition operator one obtains[22]

$$\mathscr{T}^J=\mathscr{T}^J_C+(1+\mathscr{T}^J_C\mathscr{G}^J_0)t^J(1+\mathscr{G}^J_0\mathscr{T}^J_C)\ . \tag{2.9}$$

Here $\mathscr{T}^J_C$ represents the Coulomb T operator, while $\mathscr{G}^J_0$ contains the free resolvent of the $\bar{p}$-p system

$$\mathscr{G}^J_0=\begin{bmatrix}\mathbf{G}^{\rm p}_0 & 0\\ 0 & 0\end{bmatrix} \tag{2.10}$$

with

$$\mathbf{G}^{\rm p}_0=\begin{bmatrix}G^{\rm p}_{0l_<} & 0\\ 0 & G^{\rm p}_{0l_>}\end{bmatrix} \tag{2.11a}$$

and

$$G^{\rm p}_{0L}=(E-H^{\rm p}_{0L}+i0)^{-1},\quad L=l_<,l_>\ . \tag{2.11b}$$

The operator t^J satisfies the Lippmann-Schwinger equation

$$t^J=\mathscr{V}^J_{\rm opt}+\mathscr{V}^J_{\rm opt}\mathscr{G}^Jt^J \tag{2.12}$$

with the matrix

$$\mathscr{G}^J=\begin{bmatrix}\mathbf{G}^{\rm p}_C & 0\\ 0 & \mathbf{G}^{\rm n}_0\end{bmatrix} \tag{2.13}$$

containing the $\bar{p}$-p Coulomb resolvent

$$\mathbf{G}^{\rm p}_C=\begin{bmatrix}G^{\rm p}_{Cl_<} & 0\\ 0 & G^{\rm p}_{Cl_>}\end{bmatrix}, \tag{2.14a}$$

$$G^{\rm p}_{CL}=(E-H^{\rm p}_{0L}-V_{CL}+i0)^{-1},\quad L=l_<,l_> \tag{2.14b}$$

and the free resolvent for the $\bar{n}$-n system

$$\mathbf{G}^{\rm n}_0=\begin{bmatrix}G^{\rm n}_{0l_<} & 0\\ 0 & G^{\rm n}_{0l_>}\end{bmatrix}, \tag{2.15a}$$

$$G^{\rm n}_{0L}=(E-E^{\rm n}-H^{\rm n}_{0L}+i0)^{-1},\quad L=l_<,l_>\ . \tag{2.15b}$$

The zero-energy point was chosen at $\bar{p}$-p elastic threshold so that the $\bar{n}$-n threshold is at twice the n-p mass difference

$$E^{\rm n}=2(m_{\rm n}-m_{\rm p})\ . \tag{2.16}$$

The relative momenta in either systems are

$$k^2_{\rm p}=\frac{m_{\rm p}E}{\hbar^2}\ , \tag{2.17a}$$

$$k^2_{\rm n}=\frac{m_{\rm n}}{m_{\rm p}}\left[k^2_{\rm p}-2\frac{m^2_{\rm p}}{\hbar^2}\left[\frac{m_{\rm n}}{m_{\rm p}}-1\right]\right]\ . \tag{2.17b}$$

Elastic and charge-exchange partial-wave amplitudes for $\bar{p}$-p scattering are obtained by sandwiching Eq. (2.9) between Coulombian and free asymptotic states in the following way:[22]

$$\begin{aligned}f^{\rm el}_{LL'}(E)&=-\frac{\pi m_{\rm p}}{2\hbar^2}\langle k_{\rm p}L\,\infty-|\,T^{\rm pp}_{LL'}(E+i0)\,|\,k_{\rm p}L'\,\infty+\rangle\\ &=f_{CL}(E)\delta_{LL'}\\ &\quad-\frac{\pi m_{\rm p}}{2\hbar^2}{}_C\langle k_{\rm p}L-|\,t^{\rm pp}_{LL'}(E+i0)\,|\,k_{\rm p}L'+\rangle_C\end{aligned} \tag{2.18}$$

and

$$\begin{aligned}f^{\rm ce}_{LL'}(E)&=-\frac{\pi\sqrt{m_{\rm p}m_{\rm n}}}{2\hbar^2}\langle k_{\rm n}L\,|\,T^{\rm np}_{LL'}(E+i0)\,|\,k_{\rm p}L'\,\infty+\rangle\\ &=-\frac{\pi\sqrt{m_{\rm p}m_{\rm n}}}{2\hbar^2}\langle k_{\rm n}L\,|\,t^{\rm np}_{LL'}(E+i0)\,|\,k_{\rm p}L'+\rangle_C\ .\end{aligned} \tag{2.19}$$

Here the transition operators $t^{\rm pp}_{LL'}$ and $t^{\rm np}_{LL'}$ are the partial-wave projections of the elements in

$$t^J=\begin{bmatrix}\mathbf{t}^{\rm pp} & \mathbf{t}^{\rm pn}\\ \mathbf{t}^{\rm np} & \mathbf{t}^{\rm nn}\end{bmatrix},$$

where t^{pp} and t^{np} correspond to the elastic and charge-exchange interactions $V^0_{opt}+V^1_{opt}$ and $V^0_{opt}-V^1_{opt}$, respectively. The kets $|k_pL\pm\rangle_C$ denote the Coulomb scattering states in the partial wave L.

Summing up the elastic/charge-exchange amplitudes of Eqs. (2.18) and (2.19) over all partial waves yields the spin-scattering matrices $M^S_{MM'}$ ($S=0,1$; $M,M'=-S,0,S$). The calculation of scattering observables from the spin-scattering amplitudes is extensively treated in the literature.[24] For the $\bar{p}$-p system we use formulae analogous to n-p scattering but with the inclusion of Coulomb effects.[25]

III. SEPARABLE COUPLED-CHANNEL MODEL

Our starting point is a meson-exchange model for the elastic $\bar{N}$-N interaction V^I_S. In particular we choose the real part of the Paris $\bar{N}$-N potential[5] with a cutoff

$$f(r)=\frac{\left[\frac{r}{r_0}\right]^{10}}{1+\left[\frac{r}{r_0}\right]^{10}},\quad r_0=0.8\text{ fm}\ . \tag{3.1}$$

A few remarks about this cutoff procedure are in order at this point. First of all, the meson-exchange picture is certainly not completely adequate in the range $r\lesssim 0.8$ fm. There quark-gluon dynamics can play an essential role. Equation (3.1) provides for a decrease of the meson-exchange part at small distances. This is not only demanded by high-energy phenomenology[26] but also meets the requirements of separable annihilation models.[12,13] As will be discussed in detail in the Appendix, the annihilation cross section is essentially determined by the overlap of the elastic scattering wave function with the form factor of the separable annihilation potential. In case the elastic potential shows much attraction at short distances, the corresponding wave function has a node inside the range of the annihilation form factor and thus makes the overlap integral rather small.

The elastic $\bar{N}$-N potential obtained in this manner was cast into separable form by means of the Ernst-Shakin-Thaler (EST) method.[27] This procedure, which was already successfully applied in the N-N system,[19] allowed for a fairly accurate reproduction of both the on-shell and off-shell behavior of the elastic $\bar{N}$-N interaction via the separable potential. By selecting only one or two interpolation energies per partial wave we could provide for a correct description of the $\bar{N}$-N system up to $E_{lab}\approx 150$ MeV, where special care was taken to maintain the positions of bound states and resonances especially near the elastic threshold.

The separable EST potentials in a particular partial-wave state $L,L'=J\pm 1$ with definite isospin I

$$V_{S,LL'}=\sum_{i,j=1}^{N}|g_{Li}\rangle\lambda_{ij}\langle g_{L'j}| \tag{3.2}$$

could be represented by analytic form factors of the type

$$\langle p\,|g_{Li}\rangle=g_{Li}(p)=\sum_{n=1}^{5}\frac{C_{Lin}p^L}{(p^2+\beta^2_{Lin})^{L+1}}\ . \tag{3.3}$$

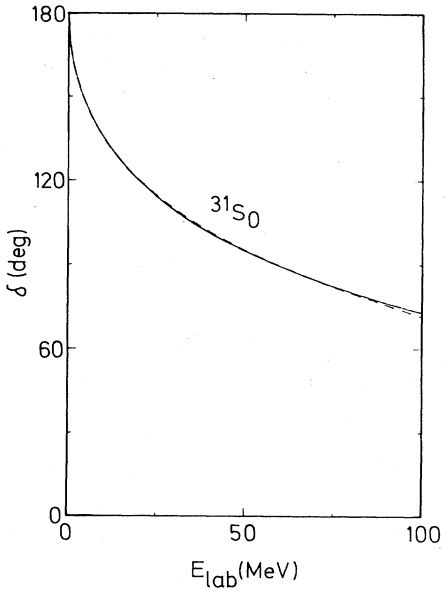

FIG. 1. Scattering phase shifts due to the elastic part of the Paris $\bar{N}$-N interaction (solid) and its separable representation (dashed).

While the potential strengths λ are determined by the EST method (for details see Ref. 18), the parameters C and β were adjusted to reproduce the half-off-shell functions up to $p\approx 6$ fm^{-1}. The numerical values are given in Table I. The quality of the on-shell and off-shell approximation is exemplified in Figs. 1 and 2.

In order to account for annihilation we added one effective two-particle decay channel per isospin. We assumed spinless and noninteracting decay products of equal mass.

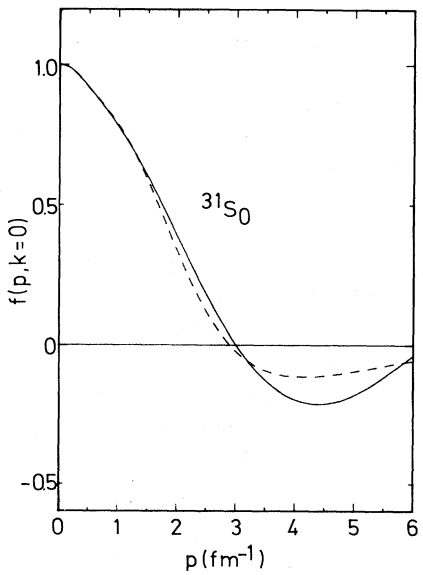

FIG. 2. Half-off-shell functions of the elastic part of the Paris $\bar{N}$-N interaction (solid) and its separable representation (dashed).

TABLE I. Parameters of the separable representation of the elastic $\bar{N}$-N interaction, Eqs. (3.2) and (3.3). Dimensions are $(C)=\mathrm{fm}^0$, $(\beta)=\mathrm{fm}^{-1}$, and $(\lambda)=\mathrm{MeV\,fm}^{-(L+L'+1)}$.

State	$I=0$		$I=1$	
	$\lambda=-1.0$		$\lambda=-1.0$	
	$\beta_1=1.0$	$C_1=-16.947\,223$	$\beta_1=1.0$	$C_1=9.401\,5746$
	$\beta_2=1.866\,066$	$C_2=19.613\,007$	$\beta_2=1.866\,066$	$C_2=-354.459\,65$
$^1S_0$	$\beta_3=2.687\,8754$	$C_3=704.609\,53$	$\beta_3=2.687\,8754$	$C_3=2489.8515$
	$\beta_4=3.482\,2022$	$C_4=-1620.0131$	$\beta_4=3.482\,2022$	$C_4=-4728.6714$
	$\beta_5=4.256\,6996$	$C_5=929.203\,64$	$\beta_5=4.256\,6996$	$C_5=2647.6517$
	$\lambda=-1.0$		$\lambda=-1.0$	
	$\beta_1=1.2$	$C_1=2.225\,4985$	$\beta_1=1.2$	$C_1=-1.224\,9177$
	$\beta_2=2.239\,2792$	$C_2=-188.924\,57$	$\beta_2=2.239\,2792$	$C_2=116.211\,12$
$^1P_1$	$\beta_3=3.225\,4504$	$C_3=2764.8436$	$\beta_3=3.225\,4504$	$C_3=-822.3519$
	$\beta_4=4.178\,6426$	$C_4=-12\,098.478$	$\beta_4=4.178\,6426$	$C_4=-1397.174$
	$\beta_5=5.108\,0396$	$C_5=12\,273.396$	$\beta_5=5.108\,0396$	$C_5=3540.5651$
	$\lambda=-1.0$		$\lambda=1.0$	
	$\beta_1=1.1$	$C_1=3.957\,071$	$\beta_1=0.8$	$C_1=-0.695\,4015$
	$\beta_2=2.2$	$C_2=-413.1827$	$\beta_2=1.6$	$C_2=110.121\,22$
$^3P_0$	$\beta_3=3.3$	$C_3=-125.861\,02$	$\beta_3=2.4$	$C_3=-613.659\,13$
	$\beta_4=4.4$	$C_4=9082.9976$	$\beta_4=3.2$	$C_4=1716.1131$
	$\beta_5=5.5$	$C_5=-12\,059.309$	$\beta_5=4.0$	$C_5=-1535.9172$
	$\lambda=1.0$		$\lambda=-1.0$	
	$\beta_1=1.4$	$C_1=47.040\,483$	$\beta_1=1.0$	$C_1=0.537\,701\,79$
	$\beta_2=3.000\,9657$	$C_2=377.987\,01$	$\beta_2=1.866\,066$	$C_2=-44.214\,116$
$^3P_1$	$\beta_3=4.687\,7173$	$C_3=-7419.3042$	$\beta_3=2.687\,8754$	$C_3=876.851\,39$
	$\beta_4=6.432\,7107$	$C_4=19\,707.559$	$\beta_4=3.482\,2022$	$C_4=-4972.9828$
	$\beta_5=8.222\,3325$	$C_5=-13\,200.458$	$\beta_5=4.256\,6996$	$C_5=5427.2397$
	$\lambda=-1.0$		$\lambda_{11}=1.0\quad\lambda_{22}=-1.0\quad\lambda_{12}=\lambda_{21}=0$	
	$\beta_1=0.8$	$C_1=0.454\,993\,29$	$\beta_{11}=1.12$	$C_{11}=15.458\,214$
	$\beta_2=1.6$	$C_2=-216.293\,02$	$\beta_{12}=2.24$	$C_{12}=-727.648\,86$
	$\beta_3=2.4$	$C_3=2188.5685$	$\beta_{13}=3.36$	$C_{13}=9023.2662$
	$\beta_4=3.2$	$C_4=-6929.309$	$\beta_{14}=4.48$	$C_{14}=-37\,749.903$
	$\beta_5=4.0$	$C_5=5396.4614$	$\beta_{15}=5.6$	$C_{15}=44\,407.618$
$^1D_2$				
			$\beta_{21}=1.12$	$C_{21}=-0.459\,475\,61$
			$\beta_{22}=2.24$	$C_{22}=308.189\,08$
			$\beta_{23}=3.36$	$C_{23}=-3426.5806$
			$\beta_{24}=4.48$	$C_{24}=-7575.8068$
			$\beta_{25}=5.6$	$C_{25}=21\,621.265$
	$\lambda=1.0$		$\lambda=-1.0$	
	$\beta_1=0.7$	$C_1=-0.297\,440\,98$	$\beta_1=0.8$	$C_1=0.203\,660\,52$
	$\beta_2=1.4$	$C_2=103.348\,26$	$\beta_2=1.6$	$C_2=-107.184\,42$
$^3D_2$	$\beta_3=2.1$	$C_3=-500.829\,19$	$\beta_3=2.4$	$C_3=945.190\,76$
	$\beta_4=2.8$	$C_4=1423.2416$	$\beta_4=3.2$	$C_4=-4415.7477$
	$\beta_5=3.5$	$C_5=-1644.1935$	$\beta_5=4.0$	$C_5=3823.5618$

State	$l_<=0$			$l_>=2$	
	$\beta_1=1.0$	$C_1=7.715\,196$	$\lambda=-1.0$	$\beta_1=1.0$	$C_1=7.704\,7071$
	$\beta_2=2.0$	$C_2=-308.805\,25$		$\beta_2=2.0$	$C_2=474.573\,31$
$^{13}S_1$-$^{13}D_1$	$\beta_3=3.0$	$C_3=1745.465$		$\beta_3=3.0$	$C_3=939.344\,74$
	$\beta_4=4.0$	$C_4=-2823.1814$		$\beta_4=4.0$	$C_4=-13\,430.2041$
	$\beta_5=5.0$	$C_5=1366.6833$		$\beta_5=5.0$	$C_5=8422.3817$

TABLE I. (*Continued*).

State	$l_<=0$			$l_>=2$	
	$\beta_1=1.2$	$C_1=-2.070\,6683$	$\lambda=-1.0$	$\beta_1=1.2$	$C_1=-5.097\,5841$
	$\beta_2=2.4$	$C_2=-29.268\,615$		$\beta_2=2.4$	$C_2=237.092\,82$
$^{33}S_1$-$^{33}D_1$	$\beta_3=3.6$	$C_3=987.271\,14$		$\beta_3=3.6$	$C_3=-4031.863$
	$\beta_4=4.8$	$C_4=-2414.2214$		$\beta_4=4.8$	$C_4=31\,567.513$
	$\beta_5=6.0$	$C_5=1484.4254$		$\beta_5=6.0$	$C_5=-41\,494.279$

State	$l_<=1$			$l_>=3$	
	$\beta_{11}=1.2$	$C_{11}=-2.920\,9933$	$\lambda_{11}=0.057\,891\,675$	$\beta_{11}=0.9$	$C_{11}=-3.218\,0388$
	$\beta_{12}=2.4$	$C_{12}=-886.599\,21$	$\lambda_{22}=1.990\,3602$	$\beta_{12}=1.8$	$C_{12}=812.177\,64$
	$\beta_{13}=3.6$	$C_{13}=1185.5683$	$\lambda_{12}=\lambda_{21}$	$\beta_{13}=2.7$	$C_{13}=18\,133.485$
	$\beta_{14}=4.8$	$C_{14}=27\,037.628$	$=0.456\,623\,12$	$\beta_{14}=3.6$	$C_{14}=77\,231.198$
	$\beta_{15}=6.0$	$C_{15}=-42\,443.332$		$\beta_{15}=4.5$	$C_{15}=-532\,171.54$
$^{13}P_2$-$^{13}F_2$					
	$\beta_{21}=1.0$	$C_{21}=25.539\,03$		$\beta_{21}=0.8$	$C_{21}=0.017\,265\,989$
	$\beta_{22}=2.0$	$C_{22}=-301.573\,98$		$\beta_{22}=1.6$	$C_{22}=-214.887\,59$
	$\beta_{23}=3.0$	$C_{23}=2205.4297$		$\beta_{23}=2.4$	$C_{33}=3527.9355$
	$\beta_{24}=4.0$	$C_{24}=-6802.3293$		$\beta_{24}=3.2$	$C_{24}=-27\,971.744$
	$\beta_{25}=5.0$	$C_{25}=6101.7597$		$\beta_{25}=4.0$	$C_{25}=54\,988.728$
	$\beta_1=1.2$	$C_1=0.115\,463\,39$	$\lambda=-1.0$	$\beta_1=1.2$	$C_1=1.850\,4198$
	$\beta_2=2.4$	$C_2=-77.924\,893$		$\beta_2=2.4$	$C_2=-1107.1985$
$^{33}P_2$-$^{33}F_2$	$\beta_3=3.6$	$C_3=978.774\,99$		$\beta_3=3.6$	$C_3=6903.702$
	$\beta_4=4.8$	$C_4=-6419.154$		$\beta_4=4.8$	$C_4=-75\,124.136$
	$\beta_5=6.0$	$C_5=8099.0724$		$\beta_5=6.0$	$C_6=61\,184.902$

State	$l_<=2$			$l_>=4$	
	$\beta_{11}=1.4$	$C_{11}=-7.790\,3969$	$\lambda_{11}=0.257\,644\,98$	$\beta_{11}=1.01$	$C_{11}=-3.804\,5573$
	$\beta_{12}=2.8$	$C_{12}=-2849.8832$	$\lambda_{22}=8.545\,2778$	$\beta_{12}=2.02$	$C_{12}=10\,042.833$
	$\beta_{13}=4.2$	$C_{13}=35\,469.711$	$\lambda_{12}=\lambda_{21}$	$\beta_{13}=3.03$	$C_{13}=-205\,483.87$
	$\beta_{14}=5.6$	$C_{14}=-39\,219.212$	$=1.905\,6356$	$\beta_{14}=4.04$	$C_{14}=2703\,774.4$
	$\beta_{15}=7.0$	$C_{15}=-14\,390.5$		$\beta_{15}=5.05$	$C_{15}=-9193\,495.7$
$^{13}D_3$-$^{13}G_3$					
	$\beta_{21}=0.98$	$C_{21}=11.486\,416$		$\beta_{21}=0.82$	$C_{21}=-0.014\,457\,158$
	$\beta_{22}=1.96$	$C_{22}=-225.319\,31$		$\beta_{22}=1.64$	$C_{22}=-320.289\,39$
	$\beta_{23}=2.94$	$C_{23}=2253.8991$		$\beta_{23}=2.46$	$C_{23}=8498.7299$
	$\beta_{24}=3.92$	$C_{24}=-8158.2281$		$\beta_{24}=3.28$	$C_{24}=-77\,982.362$
	$\beta_{25}=4.9$	$C_{25}=7907.7241$		$\beta_{25}=4.1$	$C_{25}=188\,640.32$
	$\beta_1=1.4$	$C_1=0.168\,305\,78$	$\lambda=-1.0$	$\beta_1=0.98$	$C_1=1.654\,862$
	$\beta_2=2.8$	$C_2=-336.855\,61$		$\beta_2=1.96$	$C_2=-3788.7811$
$^{33}D_3$-$^{33}G_3$	$\beta_3=4.2$	$C_3=3979.8083$		$\beta_3=2.94$	$C_3=35\,386.552$
	$\beta_4=5.6$	$C_4=-41\,360.337$		$\beta_4=3.92$	$C_4=-273\,918.41$
	$\beta_5=7.0$	$C_5=70\,694.936$		$\beta_5=4.9$	$C_5=194\,594.55$

The thresholds E^I ($I=0,1$) were put at $E_{\text{c.m.}}=-300$ MeV, which is approximately the average of the $\rho\rho$, $\omega\omega$, and $\rho\omega$ thresholds. We remark, however, that for an effective description the location of the threshold is not so crucial.

In accordance with microscopic annihilation theories[12,13] the potentials coupling to the $\bar{N}$-N decay channels were taken of separable form

$$V_{a,JL}=|g_J\rangle\kappa_{JL}\langle g_L| \tag{3.4}$$

with

$$\langle p|g_l\rangle=\frac{p^l}{(p^2+\gamma_l^2)^{l+1}},\quad l=J,L\ . \tag{3.5}$$

The separable interactions (3.2)–(3.5) constitute our $\bar{N}$-N optical potential $\mathcal{V}^J_{\text{opt}}$, which is again separable. The corresponding Lippmann-Schwinger equation (2.12) can therefore be solved by algebraic means. Also Coulomb distortion can be included rigorously. The pertinent expressions of Coulomb-distorted form factors $\langle g_{Li}|kL\pm\rangle_C$ and elements $\langle g_{Li}|G^{\text{D}}_{CL}|g_{Lj}\rangle$ are available

TABLE II. Parameters of the separable annihilation interaction, Eqs. (3.4) and (3.5). Dimensions are $(\gamma)=\mathrm{fm}^{-1}$ and $(\kappa)=\mathrm{MeV\,fm}^{-(L+J+1)}$.

	$I=0$		$I=1$	
State	κ	γ	κ	γ
$^1S_0$	2953	2.6697	3151	2.6697
$^3S_1$	44744	3.0032	40452	3.9662
$^3D_1$	31065	1.3604	25355	1.9016
$^1P_1$	1148461	4.6462	891622	4.6462
$^3P_0$	2930	1.2277	598	1.2277
$^3P_1$	120271	3.2559	174495	3.2559
$^3P_2$	18417	1.598	12313	1.598
$^1D_2$	20437	2.3685	291615	2.3685
$^3D_2$	2854507	3.1654	786487	3.1654
$^3D_3$	449447	2.09	672415	2.09

in analytic form.[22]

We designed our model for spin-singlet and triplet partial waves up to $L=2$, where angular momentum coupling was included up to $J=3$. After establishing the elastic part by means of the EST method the only parameters left open were the coupling strengths κ_{JL} and ranges γ_l ($l=J,L$) for each angular momentum L or total angular momentum J. Their values were determined by fitting the integrated elastic, charge exchange, and total cross sections at $E_{\mathrm{lab}}=50$ and 100 MeV as parametrized by Hamilton *et al.*[28] (cf. also Ref. 2). For the most important state $^3S_1$-$^3D_1$ we let the eight open parameters vary freely thus ending up with I- and L-dependent strengths and ranges. For all other partial waves the range parameters were taken to be the same in each isospin state ($I=0,1$). For the higher coupled $^3P_2$-$^3F_2$ and $^3D_3$-$^3G_3$ partial waves we allowed the annihilation to take place only in the lower angular momentum state ($^3P_2$ and $^3D_3$, respectively). The numerical values of the parameters for the annihilation potential are given in Table II.

IV. DISCUSSION

First we discuss the integrated cross sections in Fig. 3. For the total cross section σ^{tot} at low energies, in addition to the parametrization of Hamilton *et al.*,[28] there are experiments by Chaloupka *et al.*[29] and Kamae *et al.*[30] We show the results of our model calculated from the nuclear forward amplitude with Coulomb distortion. As can be seen from the upper graph in Fig. 3 there is reasonable agreement with the corresponding experimental data. For comparison we also display σ_{tot} without any Coulomb effects. The Coulomb distortion is observed to contribute significantly at smaller energies.

For the elastic cross section σ^{el} the experimental data in Fig. 3 are obtained by integration of the differential cross section measured up to $\cos\theta_{\mathrm{c.m.}}\lesssim 0.97$ omitting the pure Coulomb contribution.[29,31] Thus the data in principle contain effects from Coulomb-nuclear interference and Coulomb distortion of the nuclear amplitude. However, it is not clear how much of these effects is left out by the approximations made for the integration of differential cross section data. As in the case of σ^{tot} we show our

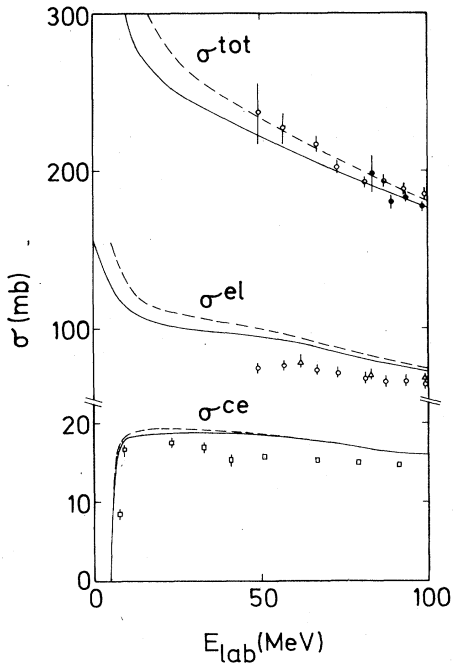

FIG. 3. Integrated cross sections of our separable model with (dashed) and without (solid) Coulomb-distortion corrections. Experimental data are taken from Ref. 28 (□), Ref. 29 (○), Ref. 30 (●), and Ref. 31 (△).

theoretical results for σ^{el} calculated from the nuclear amplitude with and without Coulomb distortion. In order to avoid ambiguities in treating the Coulomb forward singularity we excluded Coulomb-nuclear interference. In the subsequent discussion of differential cross sections it will become clear that our procedure leads to enhanced values of σ^{el}. Therefore we do not emphasize a direct comparison to experimental data but rather like to display the correct energy dependence of the integrated elastic cross section.

Our results for the integrated charge-exchange cross section σ^{ce} can be seen from the lower graph of Fig. 3. Here the effect of Coulomb distortion is not so important. The overall agreement of the Coulomb-distorted cross section with experimental data is reasonable.

Let us now turn to differential cross sections. In the low-energy domain the data base is not very large and the experiments are rather old. For our comparison we chose as examples the lowest energy available (i.e., data at $E_{\mathrm{lab}}=20$ MeV by Spencer and Edwards[32]), where we also discuss the influence of various Coulomb effects, and some moderate energy, namely, $E_{\mathrm{lab}}=62.7$ MeV. The agreement of our results with experimental data is remarkable for both energies (Fig. 4). The situation is similar at other energies up to $E_{\mathrm{lab}}\lesssim 150$ MeV. Notice that in determining the annihilation potential parameters only integrated cross sections were fitted.

For increasing energy [cf. Fig. 4(b)] we find a stronger enhancement at very forward angles (at least as compared to experimental data). However, this need not be a

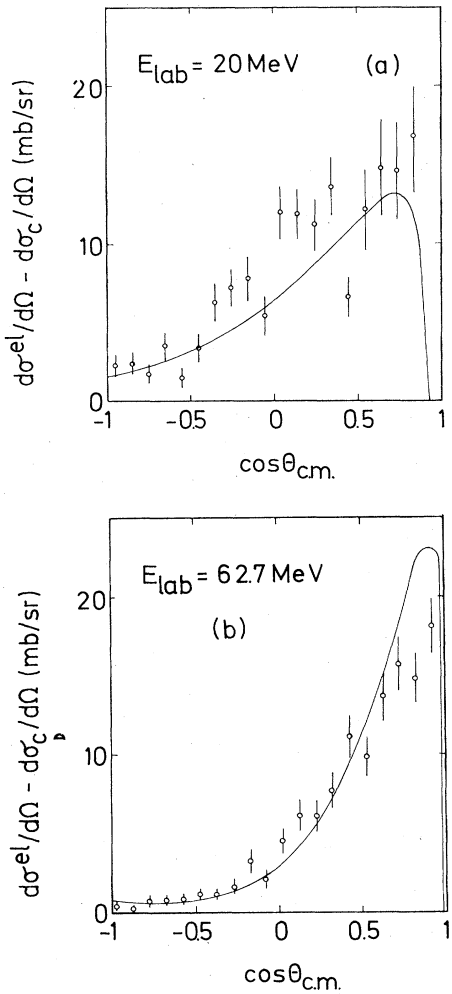

FIG. 4. Elastic differential cross sections with inclusion of Coulomb-nuclear interference and Coulomb-distortion corrections. Experimental data are taken from Ref. 32 at $E_{\rm lab}=20$ MeV and from Ref. 31 at $E_{\rm lab}=62.7$ MeV.

shortcoming of our model, since it yields the ratio of the real to the imaginary part of the spin-averaged Coulomb-distorted nuclear forward amplitude

$$\rho=\left.\frac{\mathrm{Re}(M^0_{00}+M^1_{00}+2M^1_{11})}{\mathrm{Im}(M^0_{00}+M^1_{00}+2M^1_{11})}\right|_{\theta=0} \tag{4.1}$$

rather similar to modern data[33,34] and also in close agreement with dispersion-theoretical approaches.[35] For example at $E_{\rm lab}=62.7$ MeV we obtain $\rho=-0.48$, while $\rho\approx-0.5$ is reported by Grein.[36] With respect to the ratio ρ, however, it is worthwhile to note that care has to be taken in treating spin-dependent effects. Often they were simply neglected, although they might play a significant role.[37]

For charge-exchange differential cross sections experiments are very sparse. At low energies there is only one measurement at $E_{\rm lab}=93$ MeV.[38] Our results agree reasonably well with these data (Fig. 5).

The differential cross sections just discussed were calculated under proper treatment of the long-range Coulomb interaction in connection with separable potentials.[22,25] For the results of elastic differential cross sections in Fig. 4 we subtracted the pure Coulomb cross sections; thus the Coulomb-nuclear interference and Coulomb-distortion contributions are contained. For the charge-exchange differential cross section one has only the Coulomb distortion, which is included in the results of Fig. 5. In Fig. 6 we demonstrate the role of the various Coulomb contributions and likewise of the n-p mass difference on the elastic differential cross section at $E_{\rm lab}=20$ MeV. The full line is a repetition of the curve in Fig. 4(a) and represents the exact result with inclusion of Coulomb distortion and

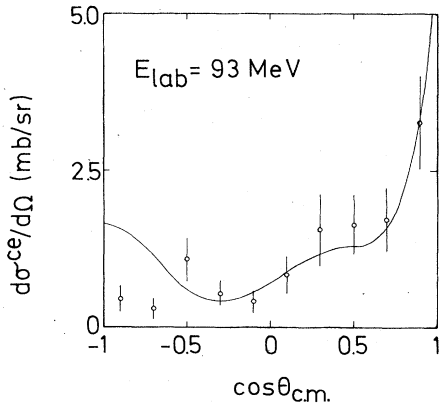

FIG. 5. Charge-exchange differential cross section with Coulomb-distortion corrections. Experimental data are taken from Ref. 38.

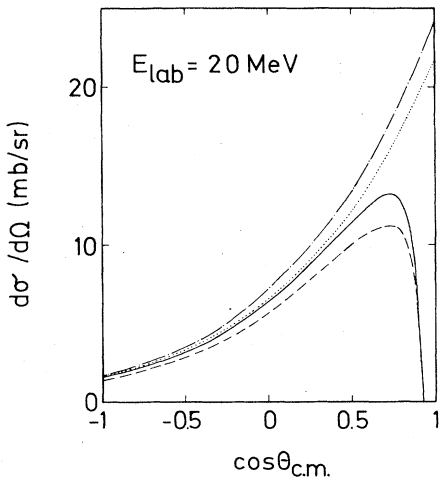

FIG. 6. Comparison of various Coulomb effects in the elastic differential cross section. The solid line is the result of Fig. 4(a), i.e., the prediction of our separable model with inclusion of Coulomb-nuclear interference and Coulomb distortion. In the dashed-dotted line Coulomb-nuclear interference is left out, the dotted line is the result without any Coulomb effects. For the dashed line Coulomb distortion was described by the approximation explained in the text; for this case also n-p mass difference effects were neglected in the thresholds.

Coulomb-nuclear interference. If the latter effect is excluded, we end up with the dashed-dotted curve. The Coulomb-distortion effect can be estimated by comparing to the purely nuclear result shown by the dotted line. In addition we quote the result (dashed curve) obtained with Coulomb-nuclear interference but by approximating the Coulomb-distortion effect by the commonly used procedure, namely, by multiplying the purely nuclear amplitude with the Coulomb phase factor $e^{2i\sigma_L}$; here, as is usually also done, we took into account the n-p mass difference only in the phase-space factors, while we neglected it in the thresholds [cf. Eq. (2.15b)]. More detailed investigations revealed that the Coulomb-distortion and n-p mass-difference effects are practically additive. The latter is much smaller and most of the defect caused by the described approximation (cf. the solid and dashed line) is due to the improper treatment of the Coulomb distortion.

Especially at low energies the Coulomb distortion is certainly not negligible. As can be seen from the comparison in Fig. 6 its effect is practically angular independent and amounts to approximately 10% at $E_{\rm lab}=20$ MeV. Therefore it is larger than in p-p scattering by a factor 2 or 3.[25] This different feature is very probably due to the influence of the $^3S_1$ state, which for $\bar{\rm p}$-p scattering additionally comes into play by the absence of the Pauli principle.

The Coulomb-nuclear interference acts destructively when added to the Coulomb-distorted nuclear cross section and causes the singular structure at forward angles (cf. the solid and dashed-dotted lines in Fig. 6). If one wants to integrate the cross section with Coulomb-nuclear interference, one has to make assumptions on the treatment of the singularity. With respect to experimental data usually a cutoff is introduced at $\cos\theta_{\rm c.m.}\approx 0.97$ and an extrapolation is employed. From the comparison of the two curves mentioned it is also clear that the integration of the Coulomb-distorted nuclear cross section without Coulomb-nuclear interference should lead to larger values of the integrated elastic cross section than in the case with interference, even if the cutoff of the forward singularity is applied. Since in our theoretical calculation in Fig. 3 we excluded Coulomb-nuclear interference, we end up with the enhanced results shown there by the dashed curve.

Finally we discuss the $\bar{\rm p}$-p threshold region. Whereas the annihilation cross section at higher energies has a $1/p$ behavior and can be parametrized by[2]

$$\sigma^{\rm ann}({\rm mb})=38+35/p_{\rm lab}\ ({\rm GeV}/c)\ , \tag{4.2}$$

it drops rapidly below this parametrization near $\bar{\rm p}$-p threshold. The appropriate quantity to study the annihilation at threshold is the product $v_{\rm c.m.}\sigma^{\rm ann}$, which becomes constant for $v_{\rm c.m.}\to 0$. Our model yields $v_{\rm c.m.}\sigma^{\rm ann}=30.4$ mb at $E_{\rm lab}=1$ MeV in close agreement with other theoretical predictions.[2] Experimentally this energy region is accessible through the measurement of hadronic level shifts of antiprotonic atoms. For example, scattering lengths and volumes can be extracted from antiprotonic hydrogen via effective-range approximations. First results from the Low Energy Antiproton Ring (LEAR) at CERN (PS 171) are now available.[39,40] For a rough estimate of the predictions of our model we quote the nuclear $1s$ and $2p$ level shifts obtained with the Trueman formula[41]

$$\Delta E(1s)=0.866a_s({\rm fm})\ {\rm keV}\ ,$$

$$\Delta E(2p)=0.0244a_{\rm p}({\rm fm}^3)\ {\rm eV}\ ,$$

where the scattering lengths are taken to be the purely nuclear ones. In Table III these level shifts are compared to the exact results from an optical model calculation,[42] where also the coupling to the $\bar{\rm n}$-n channel was included. Generally the level broadening in our model is very similar to the result of the optical potential. The level shifts, however, differ in some cases even with respect to their sign. The reason lies in the fact that in our model the annihilation depends on the particular channel and may lead to repulsive or attractive contributions for elastic scattering. On the other hand the optical potential of Ref. 42 has a state-independent annihilation with a phenomenological short-range attraction.

TABLE III. Hadronic level shifts of antiprotonic hydrogen for our separable model calculated with the Trueman formula. Comparison is given to the results of Ref. 42. See also the discussion in the text.

n	State	ΔE	ΔE (Ref. 42)
1	$^1S_0$	0.60-i0.57 keV	0.54-i0.51 keV
	$^3S_1$	0.93-i0.48 keV	0.76-i0.45 keV
2	$^1P_1$	0.002-i0.013 eV	−0.026-i0.013 eV
	$^3P_0$	0.013-i0.025 eV	−0.074-i0.056 eV
	$^3P_1$	0.038-i0.013 eV	0.036-i0.010 eV
	$^3P_2$	0.015-i0.010 eV	−0.005-i0.015 eV

V. CONCLUSION

We constructed a separable coupled-channel model for the $\bar{\rm N}$-N interaction at low and medium energies. The elastic part was derived from the meson-exchange Paris $\bar{\rm N}$-N potential in an on-shell and off-shell equivalent separable form. The coupling to the annihilation channels was described in analogy to microscopic theories by means of separable potentials. Partial waves up to $L\leq 2$ including also the couplings $^3P_2$-$^3F_2$ and $^3D_3$-$^3G_3$ were considered. Coulomb effects were taken into account rigorously.

Our model is able to reproduce the properties of $\bar{\rm p}$-p scattering up to $E_{\rm lab}\lesssim 150$ MeV in close agreement with existing phenomenological data. It has the advantage of being completely separable and should therefore be useful in a number of applications, like antinucleonic few-body calculations or in constructing optical models for the antinucleon-nucleus interaction. Since it enables one to treat the Coulomb plus hadronic interaction in an exact way, it can also facilitate more fundamental calculations of hadronic level shifts in antiprotonic atoms.

ACKNOWLEDGMENTS

We are grateful to our colleagues from the Paris group and to Dr. L. Mathelitsch for their help and many fruitful discussions. This work was supported by Fonds zur Förderung der wissenschaftlichen Forschung in Österreich, project 5234.

APPENDIX: GENERAL PROPERTIES OF SEPARABLE ANNIHILATION POTENTIALS

In the following we demonstrate some essential features of separable annihilation potentials. For simplicity the Coulomb interaction and the n-p mass difference are left out. Hence the isospin channels decouple and can be treated separately. We stay with the case of one annihilation channel with two spinless noninteracting decay particles of equal mass. Thus we have a two-channel problem, whose Hamiltonian takes the form

$$\mathscr{H}=\begin{bmatrix} H_1 & V_a^\dagger \\ V_a & H_2 \end{bmatrix}=\begin{bmatrix} \frac{\hbar^2 k_1^2}{m_1}+V_1 & V_a^\dagger \\ V_a & \frac{\hbar^2 k_2^2}{m_2}-2(m_1-m_2) \end{bmatrix} . \tag{A1}$$

Here m_1 and m_2 are the masses of the particles in the elastic (1) and decay (2) channels, respectively; k_1 and k_2 are the corresponding relative momenta. While the elastic interaction V_1 may be of arbitrary form, we now assume the annihilation potential to be separable

$$V_a=|f\rangle\lambda\langle g| . \tag{A2}$$

By using the Gell-Mann-Goldberger formalism[23] one can write the solution of the Lippmann-Schwinger equation for the transition operators in the following form:

$$\begin{bmatrix} T_{11} & T_{12} \\ T_{21} & T_{22} \end{bmatrix}=\begin{bmatrix} T_1 & 0 \\ 0 & 0 \end{bmatrix}+\begin{bmatrix} 0 & (1+V_1G_1)|g\rangle \\ |f\rangle & 0 \end{bmatrix}\begin{bmatrix} \tau_{11} & \tau_{12} \\ \tau_{21} & \tau_{22} \end{bmatrix}\begin{bmatrix} 0 & \langle f| \\ \langle g|(1+G_1V_1) & 0 \end{bmatrix} \tag{A3}$$

with the "propagators"

$$\begin{bmatrix} \tau_{11} & \tau_{12} \\ \tau_{21} & \tau_{22} \end{bmatrix}=\frac{1}{\lambda^{-2}-\langle g|G_1|g\rangle\langle f|G_2|f\rangle}\begin{bmatrix} \langle g|G_1|g\rangle & \lambda^{-1} \\ \lambda^{-1} & \langle f|G_2|f\rangle \end{bmatrix} . \tag{A4}$$

The operator $T_1=V_1+V_1G_1V_1$ belongs to the elastic channel, while G_i $(i=1,2)$ are the channel resolvents $G_i(E)=(E-H_i+i0)^{-1}$. According to this result the on-shell matrix element for the transition operator T_{21} from the elastic to the annihilation channel reads

$$\langle k_2|T_{21}(E+i0)|k_1\rangle = \frac{\langle k_2|f\rangle\lambda\langle g|k_1+\rangle}{1-\lambda^2\langle g|G_1(E)|g\rangle\langle f|G_2(E)|f\rangle} . \tag{A5}$$

Here $|k_1+\rangle$ is the scattering state corresponding to the elastic Hamiltonian H_1. The momenta are correlated by the on-shell condition

$$\hbar^2k_1^2=\frac{m_1}{m_2}\left[\hbar^2k_2^2+2m_2^2\left[1-\frac{m_1}{m_2}\right]\right]=m_1E . \tag{A6}$$

From formula (A5) several essential features of separable annihilation potentials are obvious. As a function of the coupling strength λ the annihilation cross section

$$\sigma^{\text{ann}}\propto|\langle k_2|T_{21}(E+i0)|k_1\rangle|^2$$

has a maximum for

$$\lambda^2=|\langle g|G_1(E)|g\rangle\langle f|G_2(E)|f\rangle|^{-1}$$

and vanishes for $\lambda\to 0,\infty$. For a definite λ the annihilation rate is mainly governed by the overlap of the form factor $\langle g|$ with the elastic scattering wave function $|k_1+\rangle$. Once the elastic potential is determined and the form factors (range) of the annihilation interaction are fixed, the cross section σ^{ann} can only be varied through λ. This is of importance for microscopic models ending up with separable annihilation potentials, whose form factors are restricted to a definite range. Their only open parameter is an overall coupling strength λ. If the elastic interaction is attractive leading to a node of the corresponding scattering wave function inside the range of the annihilation potential, the cross section σ^{ann} may become too small through the overlap $\langle g|k_1+\rangle$. In order to account fully for the annihilation some separable models[12] therefore require short-range elastic repulsion to increase the overlap value. By the consideration of microscopic theories for $\bar{\text{N}}$-N annihilation one may thus obtain valuable information on the elastic interaction at small distances.

In connection with optical potentials[3,9] the question is often raised whether the contribution of rescattering processes with meson-intermediate states to the elastic potential is attractive or repulsive. In the case of separable annihilation potentials it is given by the expression

$$|g\rangle\lambda^2\text{Re}(\langle f|G_2(E)|f\rangle)\langle g| ;$$

cf. the second term on the right-hand side (rhs) of Eq. (2.4b). Whether $\text{Re}\langle f|G_2(E)|f\rangle$ is positive (repulsion) or negative (attraction) depends on the range of V_a and the energy E in relation to the annihilation threshold. For the Yamaguchi-type form factors we consider [see Eq. (3.5)] it can be shown that

$$\text{Re}\langle f|G_2(E)|f\rangle\gtrless 0 \Longleftrightarrow k_2\gtrless\gamma_l . \tag{A7}$$

With the use of Eq. (A6) it follows that, if γ_l is beyond a

critical value

$$\gamma_l^{\rm crit}(E)=\frac{1}{\sqrt{2}\hbar}\left[\frac{E}{2}+m_1\right], \tag{A8}$$

rescattering can contribute only attraction. If γ_l is below this value, rescattering leads to attraction for

$$(\gamma_l^{\rm crit})^2-\gamma_l^2<\left|\frac{\sqrt{2}}{\hbar}m_2-\gamma_l^{\rm crit}\right|^2 \tag{A9}$$

and to repulsion elsewhere. For example, at $E_{\rm lab}=500$ MeV the critical value becomes $\gamma_l^{\rm crit}\approx 3.8$ fm^{-1}. If one assumes a range of the annihilation interaction of about 0.1 fm, as predicted by meson theory[9,43] the corresponding range parameter γ_l will always turn out to lie above the critical value. Consequently for short-range annihilation rescattering always leads to attraction in the optical potential.

[1] M. Lacombe *et al.*, Phys. Rev. C **21**, 861 (1980); R. Machleidt, in *Quarks and Nuclear Structure,* Proceedings of the 3rd K. Erkelenz Symposium, Bad Honnef, 1983 (Lecture Notes in Physics, Vol. 197), edited by K. Bleuler (Springer, Heidelberg, 1984); J. J. de Swart and M. M. Nagels, Fortschr. Phys. **26**, 215 (1978).

[2] C. B. Dover, Nucl. Phys. **A416**, 313c (1984); A. M. Green and J. A. Niskanen, in *Quarks and Nuclei,* edited by W. Weise (World Scientific, Singapore, 1984); B. Loiseau, Orsay Report IPNO/TH 83-44; Proceedings of the 3rd LAMPF-II Workshop, Los Alamos, 1983.

[3] C. B. Dover and J. M. Richard, Phys. Rev. C **21**, 1466 (1980); R. A. Bryan and R. J. N. Phillips, Nucl. Phys. **B5**, 201 (1968).

[4] T. Ueda, Prog. Theor. Phys. **62**, 1670 (1979).

[5] J. Côté *et al.*, Phys. Rev. Lett. **48**, 1319 (1982).

[6] M. A. Alberg *et al.*, Phys. Rev. D **27**, 536 (1983).

[7] P. H. Timmers, W. A. van der Sanden, and J. J. de Swart, Phys. Rev. D **29**, 1928 (1984).

[8] J. van Doremalen, Y. Simonov, and M. van der Velde, Nucl. Phys. **A340**, 317 (1980).

[9] B. Moussallam, Nucl. Phys. **A407**, 413 (1983).

[10] A. Faessler, G. Lübeck, and K. Shimizu, Phys. Rev. D **26**, 3280 (1982).

[11] R. Tegen, T. Mizutani, and F. Myhrer, University of South Carolina report, 1984.

[12] M. Maruyama and T. Ueda, Nucl. Phys. **A364**, 297 (1981); Phys. Lett. **124B**, 121 (1983); **149B**, 436 (1984); M. Maruyama, Prog. Theor. Phys. **69**, 937 (1983); M. Maruyama and T. Ueda, Proceedings of the International Symposium on Nuclear Spectroscopy and Nuclear Interactions, Osaka, 1984.

[13] A. M. Green, J. A. Niskanen, and J. M. Richard, Phys. Lett. **121B**, 101 (1983); A. M. Green and J. A. Niskanen, Nucl. Phys. **A412**, 448 (1984); **A430**, 605 (1984).

[14] S. Furui and A. Faessler, Nucl. Phys. **A424**, 525 (1984).

[15] S. Furui, A. Faessler, and S. B. Khadkikar, Nucl. Phys. **A424**, 485 (1984).

[16] A. M. Green, J. A. Niskanen, and S. Wycech, Phys. Lett. **139B**, 15 (1984).

[17] A. M. Green, in *Antiproton 1984, Proceedings of the VIIth European Symposium on Antiproton Interactions, Durham, 1984,* edited by M. R. Pennington (Hilger, Bristol, 1985).

[18] J. Haidenbauer and W. Plessas, Phys. Rev. C **27**, 63 (1983).

[19] J. Haidenbauer and W. Plessas, Phys. Rev. C **30**, 1822 (1984).

[20] Y. Koike, W. Plessas, and H. Zankel, University of Grar Report UNIGRAZ-UTP 2/85, 1985.

[21] A. M. Green and S. Wycech, Nucl. Phys. **A377**, 441 (1982).

[22] W. Schweiger, W. Plessas, L. P. Kok, and H. van Haeringen, Phys. Rev. C **27**, 515 (1983); **28**, 1414 (1983).

[23] M. Gell-Mann and M. L. Goldberger, Phys. Rev. **91**, 398 (1953).

[24] N. Hoshizaki, Prog. Theor. Phys. Suppl. **42**, 107 (1968); J. Bystricki, F. Lehar, and P. Winternitz, J. Phys. **39**, 1 (1978).

[25] W. Plessas, L. Mathelitsch, and F. Pauss, Phys. Rev. C **23** 1340 (1981).

[26] I. Hulthage and F. Myhrer, Phys. Rev. C **30**, 298 (1984).

[27] D. J. Ernst, C. M. Shakin, and R. M. Thaler, Phys. Rev. C **8**, 507 (1973).

[28] R. P. Hamilton, T. P. Pun, R. D. Tripp, H. Nicholson, and D. M. Lazarus, Phys. Rev. Lett. **44**, 1179 (1980); **44**, 1182 (1980).

[29] V. Chaloupka *et al.*, Phys. Lett. **61B**, 487 (1976).

[30] T. Kamae *et al.*, Phys. Rev. Lett. **44**, 1439 (1980).

[31] B. Conforto *et al.*, Nuovo Cimento **54A**, 441 (1968).

[32] D. Spencer and D. N. Edwards, Nucl. Phys. **B19**, 501 (1970).

[33] M. Cresti, L. Peruzzo, and G. Sartori, Phys. Lett. **132B**, 209 (1983).

[34] V. Ashford *et al.*, Phys. Rev. Lett. **54**, 518 (1985).

[35] H. Iwasaki *et al.*, Phys. Lett. **103B**, 247 (1981).

[36] W. Grein, Nucl. Phys. **B131**, 255 (1977).

[37] M. Lacombe, B. Loiseau, B. Moussallam, and R. Vinh Mau, Phys. Lett. **124B**, 443 (1983).

[38] R. Bizzarri *et al.*, Nuovo Cimento **54A**, 456 (1968).

[39] R. Landua, in *Antiproton 1984, Proceedings of the VIIth European Symposium on Antiproton Interactions, Durham, 1984,* edited by M. R. Pennington (Hilger, Bristol, 1985).

[40] R. Klapisch, in Particles and Nuclei, Proceedings of the 10th International Conference, Heidelberg, 1984, Nucl. Phys. **A434**, 207c (1985).

[41] T. L. Trueman, Nucl. Phys. **26**, 57 (1961).

[42] J. M. Richard and M. E. Sainio, Phys. Lett. **110B**, 349 (1982).

[43] A. Martin, Phys. Rev. **124**, 614 (1961).